 FDMP, vol.11, no.2, pp.171-195, 2015

Analysis of Natural Convection in a Nanofluid-Filled Open Cavity with a Sinusoidal Boundary Condition in the Presence of a Magnetic Field

Imen Mejri[1,2] **and Ahmed Mahmoudi**[1]

Abstract: This paper examines natural convection in an open cavity with a sinusoidal thermal boundary condition. The cavity is filled with a water-Al_2O_3 nanofluid and subjected to a magnetic field. The Lattice Boltzmann method (LBM) is applied to solve the coupled equations of flow and temperature. The study has been carried out considering parameters in the following ranges: Rayleigh number of the base fluid, Ra $= 10^3$ to 10^6, Hartmann number varied from Ha $= 0$ to 60, phase deviation ($\gamma = 0$, $\pi/4$, $\pi/2$, $3\pi/4$ and π) and solid volume fraction of nanoparticles between $\phi = 0$ and 6%. Results show that the heat transfer rate decreases with the Hartmann number and increases with Rayleigh number. At Ha $= 30$ and Ra $= 10^3$–10^5, for all phase deviations the addition of nanoparticles increases the heat transfer rate. Also, at low Rayleigh number (Ra $\leq 10^4$) the highest heat transfer rate is obtained for $\gamma = \pi/2$.

Keywords: Lattice Boltzmann Method, Magnetic field, Natural convection, Nanofluid, Phase deviation

Nomenclature

B	Magnetic field **(T)**
c	Lattice speed **(m/s)**
c_s	Speed of sound **(m/s)**
$\mathbf{c_i}$	Discrete particle speeds **(m/s)**
c_p	Specific heat at constant pressure **($\mathbf{JKg^{-1}\,K^{-1}}$)**
F	External forces **(N)**
f	Density distribution functions **($\mathbf{kg\,m^{-3}}$)**
f^{eq}	Equilibrium density distribution functions **($\mathbf{kg\,m^{-3}}$)**
g	Internal energy distribution functions **(K)**

[1] Unité de Recherche Matériaux, Energie et Energies Renouvelables (MEER), Faculté des Sciences de Gafsa, B.P.19, Zarroug, Gafsa 2112, Tunisie

[2] Corresponding Author: Imen Mejri, E-mail: im.mejri85@yahoo.fr

g^{eq}	Equilibrium internal energy distribution functions **(K)**
$\vec{g}$	Gravity vector **(m s^{-2})**
Ha	Hartmann number
k	thermal conductivity **(Wm^{-1} K^{-1})**
Ma	Mach number
n	Number of nodes
Nu	Local Nusselt number
P	Pressure **(N m^{-2})**
Pr	Prandtl number
Ra	Rayleigh number
T	Temperature **(K)**
$\mathbf{u}(u,v)$	Velocities **(m/s)**
$\mathbf{x}(x,y)$	Lattice coordinates **(m/s)**

Greek symbols

Δx	Lattice spacing **(m)**
Δt	Time increment **(s)**
τ_α	Relaxation time for temperature **(s)**
τ_ν	Relaxation time for flow **(s)**
ν	Kinematic viscosity **(m^2 s^{-1})**
α	Thermal diffusivity **(m^2 s^{-1})**
ρ	Fluid density **(kg m^{-3})**
σ	electrical conductivity **(S/m)**
ψ	Non-dimensional stream function
ϕ	Solid volume fraction
μ	Dynamic viscosity **(N s/m^2)**
γ	phase deviation

Subscript

c	cold
f	fluid
h	hot
nf	nanofluid
p	particle

1 Introduction

Magnetohydrodynamic (MHD) natural convection has received considerable attention in the recent years because of their wide variety of application in engineering

areas, such as crystal growth in liquid, cooling of nuclear reactor, electronic package, microelectronic devices, and solar technology. Because traditional fluids used for heat transfer applications such as water, mineral oils and ethylene glycol have a rather low thermal conductivity, nanofluids (homogenous suspensions of nanoparticles in a base fluid) with relatively higher thermal conductivities due to the high thermal conductivity of the nanoparticles, have attracted enormous interest from researchers due to their potential in enhancement of heat transfer. **[Khanafer, Vafai & Lightstone (2003)]** investigated numerically natural convection heat transfer in a two-dimensional vertical enclosure utilizing nanofluids. It was revealed that the heat transfer rate increases with the increase of particle fraction at any given Grashof number. **[Jahanshahi, Hosseinizadeh, Alipanah, Dehghani & Vakilinejad (2010)]** studied natural convection of water-SiO_2 nanofluid using two different models, in the first model they have employed a set of experimental data for thermal conductivity of nanofluid and in the second model they have calculated the thermal conductivity using the theoretical formulations. Their results showed an enhancement in thermal conductivity due to the adding of nanoparticles at both models. **[Ghasemi, Aminossadati & Raisi (2011)]** examined natural convection in an enclosure that is filled with a water-Al_2O_3 nanofluid and is influenced by a magnetic field. The found results show that the heat transfer rate increases with an increase of the Rayleigh number but it decreases with an increase of the Hartmann number. Also an increase of the solid volume fraction may result in enhancement or deterioration of the heat transfer performance depending on the value of Hartmann and Rayleigh numbers. **[Fattahi, Farhadi, Sedighi & Nemati (2012)]** applied Lattice Boltzmann Method to investigate the natural convection flows utilizing nanofluids in a square cavity. The fluid in the cavity was a water-based nanofluid containing Al_2O_3 or Cu nanoparticles. The results indicated that by increasing solid volume fraction, the average Nusselt number increased for both nanofluids. It was found that the effects of solid volume fraction for Cu were stronger than Al_2O_3. **[Kefayati, Hosseinizaeh, Gorji, Sajjadi (2011)]** simulated by the Lattice Boltzmann method the natural convection in enclosures using water/SiO_2 nanofluid. The results showed that the average Nusselt number increased with volume fraction for the whole range of Rayleigh numbers and aspect ratios. Also the effect of nanoparticles on heat transfer augmented as the enclosure aspect ratio increased. **[Mahmoudi, Mejri, Abbassi & Omri (2013)]** applied the double-population Lattice Boltzmann Method to solve the natural convective problem in an inclined triangular cavity filled with air, two different boundary conditions are implemented. Comparison with previously published results shows excellent agreement. also It is observed that inclination angle can be used as a relevant parameter to control heat transfer in a triangular cavity. **[Sheikholeslami, Gorji-Bandpy, Ganji & Soleimani (2014)]** investigated free convection heat transfer in an enclosure filled

with nanofluid, the effects of Brownian motion and thermophoresis have been included in the model of nanofluid. **[Mejri, Mahmoudi, Abbassi & Omri (2014 a)]** studied the laminar natural convection and entropy generation in a square enclosure, with sinusoidal temperature distribution, filled with a water-Al_2O_3 nanofluid and is subjected to a magnetic field. **[Mahmoudi, Mejri, Abbassi & Omri (2014 a)]** studied the effect of magnetic field and it direction on water-Al_2O_3 nanofluid filled cavity with a linear boundary condition, they exhibited that the magnetic field direction has effects on the flow and heat transfer rates in the cavity. **[Kefayati (2013)]** applied lattice Boltzmann method to simulate heat dissipation effect of a ferrofluid on natural convection flow at the presence of an external magnetic source. The cavity is filled with kerosene as the carrier fluid and nanoscale ferromagnetic particle of cobalt. **[Mejri, Mahmoudi, Abbassi & Omri (2014 b)]** studied the laminar natural convection in a square enclosure, with non-uniform heating on both side walls, filled with a water-Al_2O_3 nanofluid and is subjected to a magnetic field. The found results show that the heat transfer rate increases with an increase in the Rayleigh number but it decreases with an increase in the Hartmann number. **[Quere, Humphrey & Sherman (1981)]** investigated open isothermal square cavities using aspect ratio of unity. Chan et al. **[Chan & Tien (1985)]** essayed a numerical study on an open square enclosure with isothermal heated side and adiabatic top and bottom walls. **[Mohamad (1995)]** studied isothermal inclined open cavities with aspect ratios of 0.5–2. **[Mohamad, Ganaoui & Bennacer (2009)]** studied natural convection in an open enclosure numerically with Lattice Boltzmann method. They investigated the effects of systematic analysis of aspect ratio on the physics of the flow and heat transfer. They have showed that increasing the aspect ratio for a given Rayleigh number decreases the rate of heat transfer up to the conduction limit. **[Mahmoudi, Shahi, Shahedin & Hemati (2011)]** investigated numerical modeling of natural convection in an open enclosure with two vertical thin heat sources subjected to a nanofluid. They demonstrated that the average Nusselt number increases linearly with the increase in the solid volume fraction of nanoparticles. **[Mohamad, Bennacer & Ganaoui (2010)]** studied double dispersion in an open end cavities using Lattice Boltzmann Method. **[Kefayati, Hosseinizadeh, Gorji & Sajjadi (2012)]** studied natural convection in an open enclosure which subjugated to water/copper nanofluid using Lattice Boltzmann Method. the found results show that the average Nusselt number increases with augmentation of Rayleigh number and the volume fraction of nanoparticles. Also, the average Nusselt number decreases as the aspect ratio increases at various Rayleigh numbers and different the nanoparticle volume fractions. **[Mahmoudi, Mejri, Abbassi & Omri (2014 b)]** studied the MHD natural convection on nanofluid filled open cavity with non uniform boundary condition in the presence of uniform heat generation/absorption. The results show that the nanoparticles effect is more im-

portant for heat generation condition than absorption generation condition.

The aim of the present study is to investigate numerically the heat transfer rate and the fluid flow in a nanofluid filled open cavity with a sinusoidal boundary condition and subjected to a magnetic field. Lattice Boltzmann method (LBM) is applied to solve the coupled equations of flow and temperature fields. The LBM results are validated with previous numerical investigations and the effects of the main parameters (Rayleigh number, Hartmann number, phase deviation and solid volume fraction) on flow and thermal fields are researched.

2 Mathematical formulation

2.1 Problem statement

The geometry of the present problem is shown in **Fig. 1**. It displays a two-dimensional cavity with the height of H. A sinusoidal temperature is imposed along the left vertical wall. An external cold nanofluid enters into the enclosure from the east opening boundaries while the Al_2O_3–water nanofluid is correlated with the opening boundary at the constant temperature of T_c. The top and bottom horizontal walls have been considered to be adiabatic. A magnetic field with uniform strength B_0 is applied in the horizontal direction. The nanofluid is Newtonian and incompressible. The flow is considered to be steady, two dimensional and laminar, and the radiation effects are negligible. The base fluid and the nanoparticles are in thermal equilibrium, the nanofluids were assumed to be similar to a pure fluid and then nanofluid qualities were gotten and they were applied for the equations of the considered problem. The thermo-physical properties of the base fluid and the nanoparticles are given in **Table 1**. The density variation in the nanofluid is approximated by the standard Boussinesq model. It is assumed that the induced magnetic field produced by the motion of an electrically conducting fluid is negligible compared to the applied magnetic field. Furthermore, it is assumed that the viscous dissipation and Joule heating are neglected.

Table 1: Thermo-physical properties of water and nanoparticles

	ρ (kg /m^3)	C_p (J/kg K)	K (W/mK)	β (K^{-1})
Pure water	997.1	4179	0.613	$21\text{x}10^{-5}$
Al_2 O_3	3970	765	40	$0.85\text{x}10^{-5}$

Therefore, governing equations can be written in dimensional form as follows:

$$\frac{\partial u}{\partial x}+\frac{\partial v}{\partial y}=0 \tag{1}$$

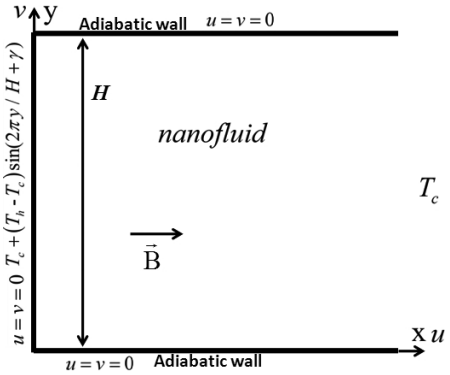

Figure 1: Geometry of the present study with boundary conditions

$$\rho_{nf}(u\frac{\partial u}{\partial x}+v\frac{\partial u}{\partial y})=-\frac{\partial p}{\partial x}+\mu_{nf}(\frac{\partial^2 u}{\partial x^2}+\frac{\partial^2 u}{\partial y^2}) \tag{2}$$

$$\rho_{nf}(u\frac{\partial v}{\partial x}+v\frac{\partial v}{\partial y})=-\frac{\partial p}{\partial y}+\mu_{nf}(\frac{\partial^2 v}{\partial x^2}+\frac{\partial^2 v}{\partial y^2})+F_y \tag{3}$$

$$u\frac{\partial T}{\partial x}+v\frac{\partial T}{\partial y}=\alpha_{nf}(\frac{\partial^2 T}{\partial x^2}+\frac{\partial^2 T}{\partial y^2}) \tag{4}$$

Where F_y is the total body forces at y direction and it is defined as follows:

$$F_y=-\frac{Ha^2\mu_{nf}}{H^2}v+(\rho\beta)_{nf}g(T-T_m) \tag{5}$$

With

$$Ha=HB_0\sqrt{\frac{\sigma_{nf}}{\mu_{nf}}} \tag{6}$$

The classical models reported in the literature are used to determine the properties of the nanofluid **[Xuan & Roetzel (2000)]**:

$$\rho_{nf}=(1-\phi)\rho_f+\phi\rho_p \tag{7}$$

$$(\rho c_p)_{nf}=(1-\phi)(\rho c_p)_f+\phi(\rho c_p)_p \tag{8}$$

$$(\rho\beta)_{nf}=(1-\phi)(\rho\beta)_f+\phi(\rho\beta)_p \tag{9}$$

$$\alpha_{nf}=\frac{k_{nf}}{(\rho c_p)_{nf}} \tag{10}$$

In the above equations, ϕ is the solid volume fraction, ρ is the density, σ is the electrical conductivity, α is the thermal diffusivity, c_p is the specific heat at constant pressure and β is the thermal expansion coefficient. The viscosity of the nanofluid

containing a dilute suspension of small rigid spherical particles and the thermal conductivity of the nanofluid can be modelled by **[Brinkman (1956) & Maxwell (1873)]**:

$$\mu_{nf} = \frac{\mu_f}{(1-\phi)^{2.5}} \tag{11}$$

$$k_{nf} = k_f \frac{k_P + 2k_f - 2\phi(k_f - k_P)}{k_P + 2k_f + \phi(k_f - k_P)} \tag{12}$$

The governing equations are subject to the following boundary conditions:

$$\text{Bottom wall } u = v = 0 \quad \left.\frac{\partial T}{\partial y}\right|_{y=0} = 0 \tag{13}$$

$$\text{Top wall } u = v = 0 \quad \left.\frac{\partial T}{\partial y}\right|_{y=H} = 0 \tag{14}$$

$$\text{Left wall } u = v = 0 \quad T(0,y) = T_C + (T_h - T_c)\sin(2\pi\frac{y}{H} + \gamma) \tag{15}$$

$$\text{Right wall } \begin{cases} \text{if } u > 0 \text{ then } \left.\dfrac{\partial T}{\partial x}\right|_{x=H} = 0 \\ \text{if } u < 0 \text{ then } T(H,y) = T_c \end{cases} \tag{16}$$

2.2 Simulation of MHD and nanofluid with Lattice Boltzmann Method

For the incompressible non isothermal problems, Lattice Boltzmann Method (LBM) utilizes two distribution functions, f and g, for the flow and temperature fields respectively.

For the flow field:

$$f_i(\mathbf{x} + \mathbf{c_i}\Delta t, t + \Delta t) = f_i(\mathbf{x}, t) - \frac{1}{\tau_v}\left(f_i(\mathbf{x}, t) - f_i^{\text{eq}}(\mathbf{x}, t)\right) + \Delta t F_i \tag{17}$$

For the temperature field:

$$g_i(\mathbf{x} + \mathbf{c_i}\Delta t, t + \Delta t) = g_i(\mathbf{x}, t) - \frac{1}{\tau_\alpha}\left(g_i(\mathbf{x}, t) - g_i^{\text{eq}}(\mathbf{x}, t)\right) \tag{18}$$

Where the discrete particle velocity vectors defined by $\mathbf{c_i}$, Δt denotes lattice time step which is set to unity. τ_v, τ_α are the relaxation time for the flow and temperature fields, respectively. f_i^{eq}, g_i^{eq} are the local equilibrium distribution functions that have an appropriately prescribed functional dependence on the local hydrodynamic properties which are calculated with Eqs. (19) and (20) for flow and temperature fields respectively.

$$f_i^{\text{eq}} = \omega_i \rho \left[1 + \frac{3(\mathbf{c_i}.\mathbf{u})}{c^2} + \frac{9(\mathbf{c_i}.\mathbf{u})^2}{2c^4} - \frac{3\mathbf{u}^2}{2c^2}\right] \tag{19}$$

$$g_i^{\mathrm{eq}} = \omega_i' T \left[1 + 3\frac{\mathbf{c_i}.\mathbf{u}}{c^2}\right] \tag{20}$$

$\mathbf{u}$ and ρ are the macroscopic velocity and density, respectively. c is the lattice speed which is equal to $\Delta x/\Delta t$ where Δx is the lattice space similar to the lattice time step Δt which is equal to unity, ω_i is the weighting factor for flow, ω_i' is the weighting factor for temperature. D2Q9 model for flow and D2Q4 model for temperature are used in this work so that the weighting factors and the discrete particle velocity vectors are different for these two models and they are calculated with Eqs (21–23) as follows:

For D2Q9

$$\omega_0 = \frac{4}{9}, \omega_i = \frac{1}{9} \text{ for } i = 1,2,3,4 \text{ and } \omega_i = \frac{1}{36} \text{ for } i = 5,6,7,8 \tag{21}$$

The discrete velocities for the D2Q9 are defined as follows:

$$\mathbf{c_i} = \begin{cases} 0 & i = 0 \\ (\cos[(i-1)\,\pi/2], \sin[(i-1)\pi/2])c & i = 1,2,3,4 \\ \sqrt{2}\,(\cos[(i-5)\,\pi/2+\pi/4], \sin[(i-5)\pi/2+\pi/4])\,c & i = 5,6,7,8 \end{cases} \tag{22}$$

For D2Q4

The temperature weighting factor for each direction is equal to $\omega_i' = 1/4$.

The discrete velocities for the D2Q4 are defined as follows:

$$\mathbf{c_i} = (\cos[(i-1)\,\pi/2], \sin[(i-1)\pi/2])c \quad i = 1,2,3,4 \tag{23}$$

The kinematic viscosity ν and the thermal diffusivity α are then related to the relaxation time by Eq. (24):

$$\nu = \left[\tau_\nu - \frac{1}{2}\right] c_s^2 \Delta t \quad \alpha = \left[\tau_\alpha - \frac{1}{2}\right] c_s^2 \Delta t \tag{24}$$

Where c_s is the lattice speed of sound witch is equals to $c_s = c/\sqrt{3}$. In the simulation of natural convection, the external force term F appearing in Eq. (17) is given by Eq. (25)

$$F_i = \frac{\omega_i}{c_s^2} F.c_i \tag{25}$$

Where $F = F_y$.

The macroscopic quantities, $\mathbf{u}$ and T can be calculated by the mentioned variables, with Eq. (26–28).

$$\rho = \sum_i f_i \tag{26}$$

$$\rho \mathbf{u} = \sum_i f_i \mathbf{c_i} \tag{27}$$

$$T = \sum_i g_i \tag{28}$$

2.3 Boundary conditions

The implementation of boundary conditions is very important for the simulation. The distribution functions out of the domain are known from the streaming process. The unknown distribution functions are those toward the domain.

2.3.1 Flow

Bounce-back boundary conditions were applied on all solid boundaries, which mean that incoming boundary populations are equal to out-going populations after the collision. At the east open boundary, the following condition is used:

$$f_{6,n} = f_{6,n-1}, f_{3,n} = f_{3,n-1} \text{ and } f_{7,n} = f_{7,n-1} \tag{29}$$

2.3.2 Temperature

The bounce back boundary condition is used on the adiabatic wall. Temperature at the west and east walls are known. Since we are using D2Q4, the unknown internal energy distribution functions are evaluated as:

$$\text{Right wall: } \begin{cases} \text{if } u > 0 \text{ then } g_{3,n} = g_{3,n-1} \\ \text{if } u < 0 \text{ then } g_3 = T_c - g_1 - g_2 - g_4 \end{cases} \tag{30}$$

$$\text{Left wall: } g_1 = T(y) - g_2 - g_3 - g_4 \tag{31}$$

2.4 Non-dimensional parameters

By fixing Rayleigh number, Prandtl number and Mach number, the viscosity and thermal diffusivity are calculated from the definition of these non dimensional parameters.

$$\nu_f = N.Ma.c_s \sqrt{\frac{\text{Pr}}{Ra}} \tag{32}$$

Where N is number of lattices in y-direction. Rayleigh and Prandtl numbers are defined as $Ra = \frac{g\beta_f H^3 (T_h - T_c)}{\nu_f \alpha_f}$ and $\text{Pr} = \frac{\nu_f}{\alpha_f}$, respectively. Mach number should be less than $Ma = 0.3$ to insure an incompressible flow. Therefore, in the present study, Mach number was fixed at $Ma = 0.1$. Nusselt number is one of the most

important dimensionless parameters in the description of the convective heat transport. The local Nusselt number (Nuy), the average Nusselt number (Nu) and the dimensionless average Nusselt number (Nu*) on the left wall are calculated as:

$$Nuy = -\frac{k_{nf}}{k_f}\frac{H}{T_h - T_c}\frac{\partial T}{\partial x}\bigg|_{x=0} \tag{33}$$

$$Nu = \frac{1}{H}\int_{heating\ half} Nuydy \tag{34}$$

$$Nu^*(\phi) = \frac{Nu(\phi)}{Nu(\phi = 0)} \tag{35}$$

Table 2: Comparison of average Nusselt number at hot wall.

Ra	present	LBM [**Mohamad et al. (2009)**]	FVM [**Mohamad (1995)**]
10^4	3.250	3.377	3.264
10^5	7.237	7.323	7.261
10^6	14.222	14.380	14.076

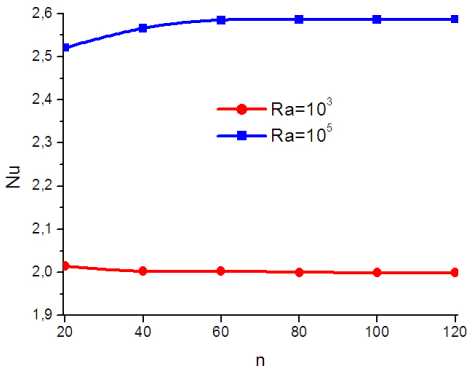

Figure 2: Average Nusselt number on the hot wall for different uniform grids ($\gamma = \pi/2$, Ha $= 0$ and $\phi = 0$)

3 Validation of the numerical code:

Lattice Boltzmann Method scheme was utilized to obtain the numerical simulations in an open cavity with a sinusoidal boundary condition filled with water/Al_2O_3 nanofluid and submitted to a magnetic field. **Fig. 2** demonstrates the effect of grid resolution and the lattice sizes (20x20), (40x40), (60x60), (80x80), (100x100) and

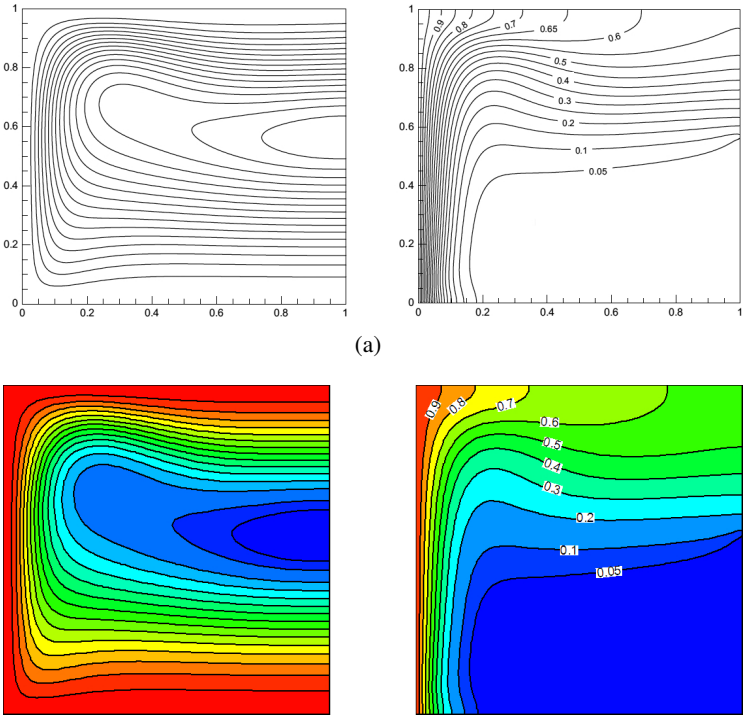

Figure 3: Comparison of the streamlines and isotherms for Ra $= 10^5$ and Pr $= 0.7$ between (a) numerical results by **[Mohamad, Ganaoui & Bennacer (2009)]** and (b) the present result

(120x120) for Ha $= 0$ and $\phi = 0$ by calculating the average Nusselt number for Ra $= 10^3$ and 10^5, it was found that a grid size of (100x100) ensures a grid independent solution. In order to check on the accuracy of the numerical technique employed for the solution of the considered problem, the present numerical code was validated with the published study of **[Mohamad, Ganaoui & Bennacer (2009)]** for the same cavity for Ra $= 10^5$ and Pr $= 0.7$. The results are presented in **Fig.3**, the streamlines and isotherms have a good agreement between both compared results. **Table 2** shows the comparison of average Nusselt number at hot wall of present study with prediction of LBM **[Mohamad, Ganaoui & Bennacer (2009)]** and Finite Volume Method (FVM) **[Mohamad (1995)]**. These comparisons show that the present study has a good agreement with previous studies. Another validation with results by **[Khanafer, Vafai & Lightstone (2003)]** and **[Jahanshahi, Hosseinizadeh, Alipanah, Dehghani & Vakilinejad (2010)]**for natural convection in an enclosure filled with water/Cu nanofluid for Ra $= 6.2\text{x}10^5$ and $\phi = 0.1$

as shown in **Fig.4**, excellent agreement is also found. The present code is also validated with the results of **[Ghasemi, Aminossadati & Raisi (2011)]** at the presence of nanofluid and magnetic filed (**Fig. 5**), it shows the dimensionless temperature along the horizontal axial midline of the enclosure for three values of the Hartmann number, for Ra $= 10^5$ and for a solid volume fraction $\phi = 0.03$, **Fig. 5** shows good agreement between the present code and the published results.

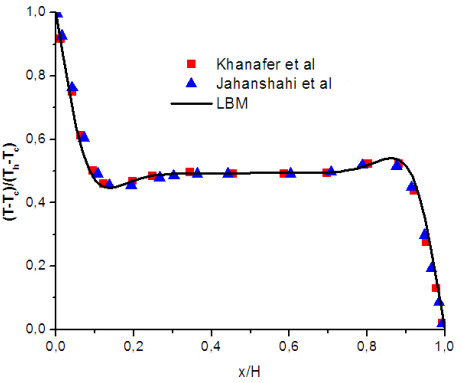

Figure 4: Comparison of the temperature on axial midline between the present results and numerical results by **[Khanafer, Vafai & Lightstone (2003)]** and **[Jahanshahi, Hosseinizadeh, Alipanah, Dehghani & Vakilinejad (2010)]** (Pr $= 6.2$, $\phi = 0.1$, Gr $= 10^4$)

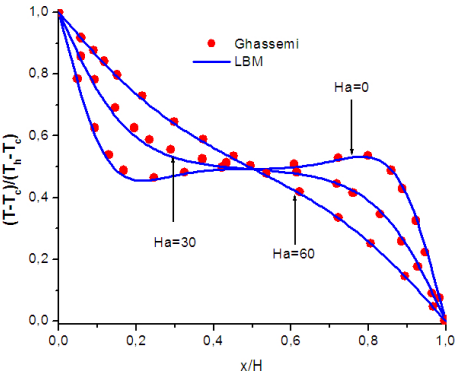

Figure 5: Comparison of the temperature on axial midline between the present results and numerical results by **[Ghasemi, Aminossadati & Raisi (2011)]** ($\phi = 0.03$, Ra $= 10^5$)

4 Results and discussion

4.1 Effect of Hartmann and Rayleigh numbers

Fig. 6–7 illustrate the effect of Rayleigh number for three values of Hartmann number (Ha $= 0$, 50 and 100) and for $\gamma = \pi/2$ on the isotherms and streamlines of nanofluid ($\phi = 0.04$) and pure fluid ($\phi = 0$). It is shown that the thickness of the boundary layer at the left wall increases with Hartmann number and decreases with Rayleigh number. Therefore the temperature gradient and subsequently heat transfer increases with Rayleigh numbers and decreases with Hartmann numbers. For the streamlines, in the absence of the magnetic field, for low Rayleigh number (Ra $\leq 10^4$) the flow is characterized by a main driven anticlockwise flow circulation occupying the cavity, weak cells may develop at the corners of the cavity, the cells

intensity increases with Rayleigh number. For high Rayleigh number (Ra $\geq 10^5$), the cell at the top of the cavity is transformed to a secondary driven clockwise flow circulation occupying the upper region of the cavity. In the presence of the magnetic field, the fluid flow intensity decreases with Hartmann number, whereas the size of the secondary cells increases with the Hartmann number.

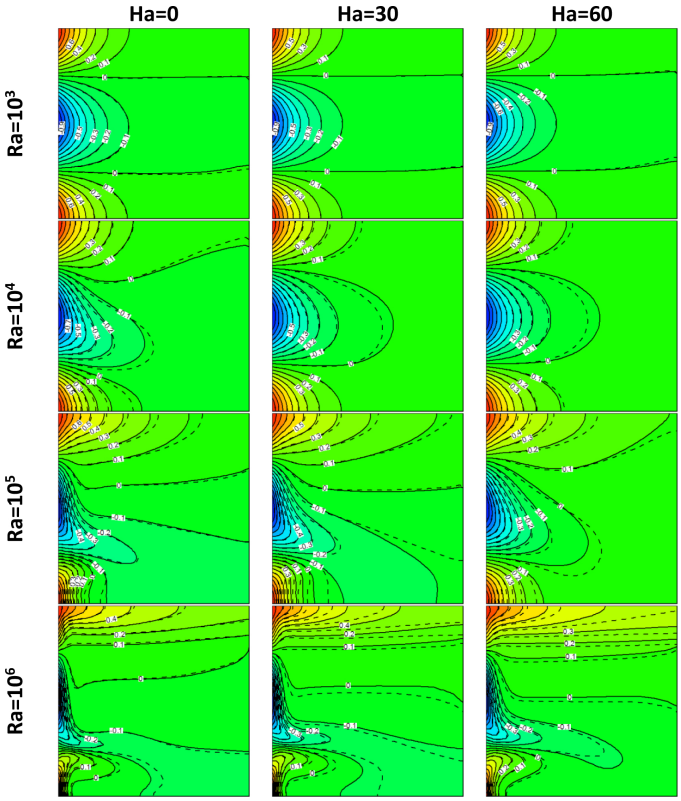

Figure 6: Isotherms for different Hartmann and Rayleigh numbers for $\gamma = \pi/2$, (—) $\phi = 0.04$ and (- - -) $\phi = 0$

Fig.8 shows the variation of average Nusselt number as function of Hartmann number at different Rayleigh number for $\gamma = \pi/2$ and $\phi = 0$. It is observed that the increase of Rayleigh number increases the heat transfer rate, on the contrary, the increase of the Hartmann number decreases the heat transfer rate. For low Rayleigh number (Ra $\leq 10^4$) the heat transfer rate is constant for all values of Hartmann number, the conduction is dominant. For Ra $\geq 10^5$, the heat transfer rate decreases with Hartmann number, indicating that the convection is more and more disadvantaged with the Hartmann number.

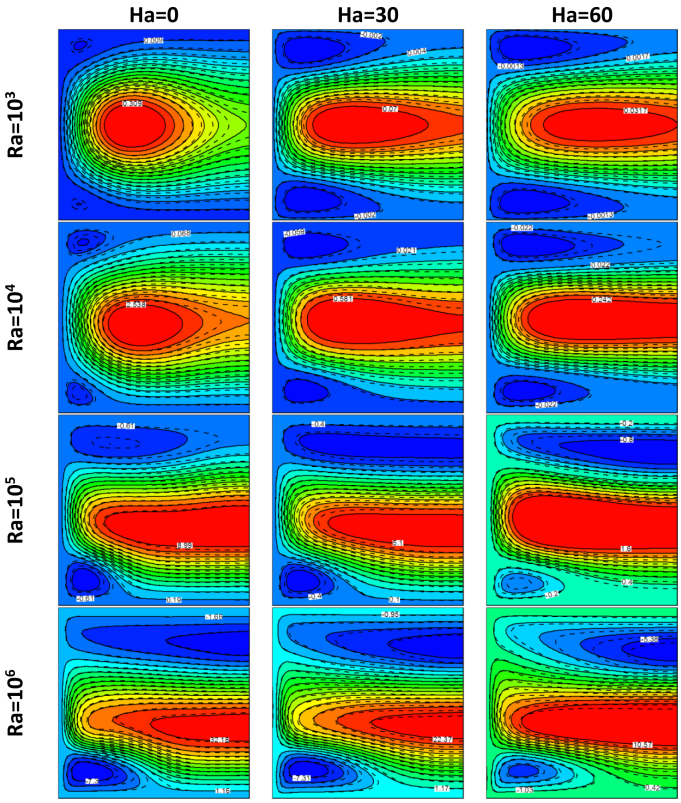

Figure 7: Streamlines for different Hartmann and Rayleigh numbers for $\gamma = \pi/2$, (—) $\phi = 0.04$ and (- - -) $\phi = 0$

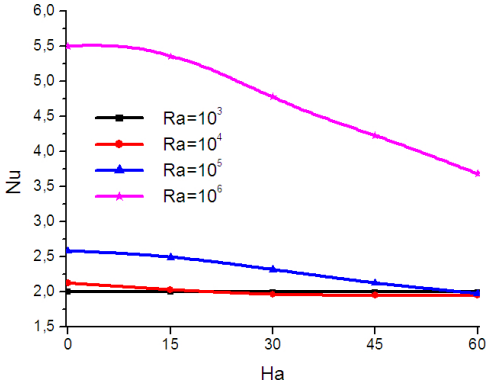

Figure 8: Variation of the average Nusselt number with Hartmann number for different Rayleigh number for $\gamma = \pi/2$ and $\phi = 0$

Fig. 9a–b show the local Nusselt number on the left wall respectively for Ha = 0 and 60 for several Rayleigh number at $\gamma = \pi/2$ and $\phi = 0$. For both cases, the local Nusselt number increases with Rayleigh number. The curves drawn for the Nusselt numbers against y/H are approximately of sinusoidal shape like the thermal boundary. This indicates that the local heat transfer is directly affected by the temperature distribution on the surface. In other words, larger heat transfer occurs when the temperature is higher.

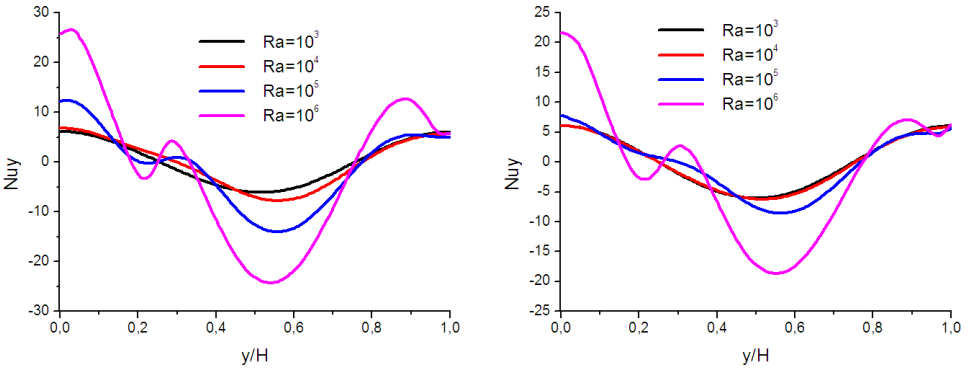

Figure 9: Variation of the local Nusselt number on the left wall for different Rayleigh number for (a) Ha = 0 and (b) Ha = 60 for $\gamma = \pi/2$ and $\phi = 0$

Fig. 10a–b show the local Nusselt number on the left wall respectively for Ra = 10^4 and 10^5 for several Hartmann number at $\gamma = \pi/2$ and $\phi = 0$. For both cases, the local Nusselt number decreases with Hartmann number. For Ra = 10^4 the heat transfer gets no remarkable change by varying the Hartmann number, the opposite is true for Ra = 10^5. The magnetic field effect is more significant for high Rayleigh number.

4.2 Phase deviation effect

Fig. 11–12 illustrate the Hartmann number effect (Ha = 0, 30 and 60) for different phase deviation ($\gamma = 0$, $\pi/4$, $\pi/2$, $3\pi/2$ and π) and for Ra = 10^3 on the isotherms and streamlines of nanofluid ($\phi = 0.04$) and pure fluid ($\phi = 0$). For all phase deviation it is shown that the effect of nanoparticles on the isotherms decreases with the augmentation of Hartmann number. Isotherms are regularly distant indicating that the conductive regime is dominant. Streamlines show that the phase deviation affects the flow through the cavity, for all phase deviation, the flow intensity decreases with Hartmann number. For $\gamma = 0$, two symmetric main flows occupying the cavity and flowing in the opposite directions are formed. The flow at the

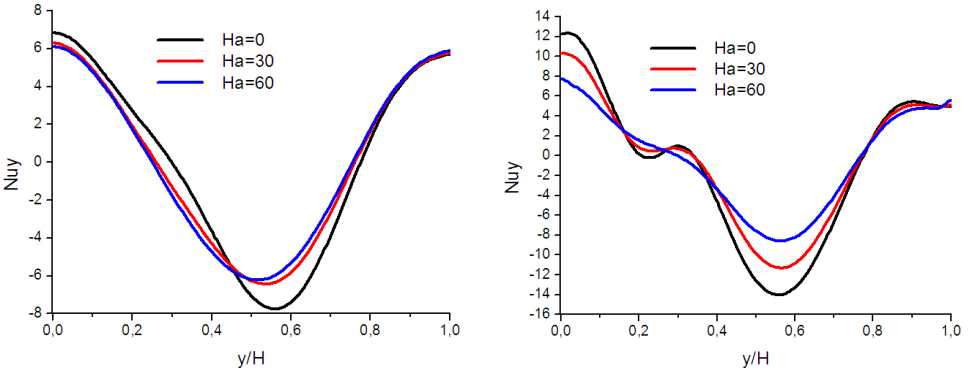

Figure 10: Variation of the local Nusselt number on the left wall for different Hartmann number for (a) Ra $= 10^4$ and (b) Ra $= 10^5$ for $\gamma = \pi/2$ and $\phi = 0$

bottom of the cavity is clockwise, while the flow at the top of the cavity is in the counterclockwise direction (The opposite directions for $\gamma = \pi$). The increase of Hartmann does not break the symmetry but slows the flow. For $\gamma = \pi/4$, A main flow occupying the majority of the cavity and flowing in the counterclockwise is formed. A weak cell is formed at the bottom corner of the cavity (at the top corner of the cavity for $\gamma = 3\pi/4$) which the size increases with the Hartmann number, order to ensure a flow through the cavity in the clockwise direction.

Fig. 13–14 illustrate the Hartmann number effect (Ha $= 0$, 30 and 60) for different phase deviation ($\gamma = 0$, $\pi/4$, $\pi/2$, $3\pi/2$ and π) and for Ra $= 10^5$ on the isotherms and streamlines of nanofluid ($\phi = 0.04$) and pure fluid ($\phi = 0$). For all phase deviation, it is shown that the thickness of the boundary layer at the left wall increases with Hartmann number. Therefore the temperature gradient and subsequently heat transfer decreases with Hartmann numbers. For $\gamma = 0$ (respectively $\gamma = \pi/4$) and Ha $= 0$, A main flow occupying the majority of the cavity and flowing in the clockwise (counterclockwise) is formed. A cell exists at the top (bottom) corner of the cavity which the size increases with the Hartmann number, order to ensure a flow through the cavity in the counterclockwise (clockwise) direction. For $\gamma = 3\pi/4$ (respectively $\gamma = \pi$) two main flows occupying the cavity and flowing in the opposite directions are formed. The flow at the bottom of the cavity is counterclockwise, while the flow at the top of the cavity is in the clockwise direction.

Fig.15 shows the variation of the average Nusselt number as function of Hartmann number at different phase deviation for Ra $= 10^5$ and $\phi = 0$. For all phase deviation, it is observed that the increase of Hartmann number decreases the heat transfer rate. For $\gamma \geq \pi/2$, the heat transfer rate increases with the phase deviation. For Ha $= 0$, the heat transfer rate is the same for $\gamma = 0$ and π, also for $\gamma = \pi/4$ and $3\pi/4$.

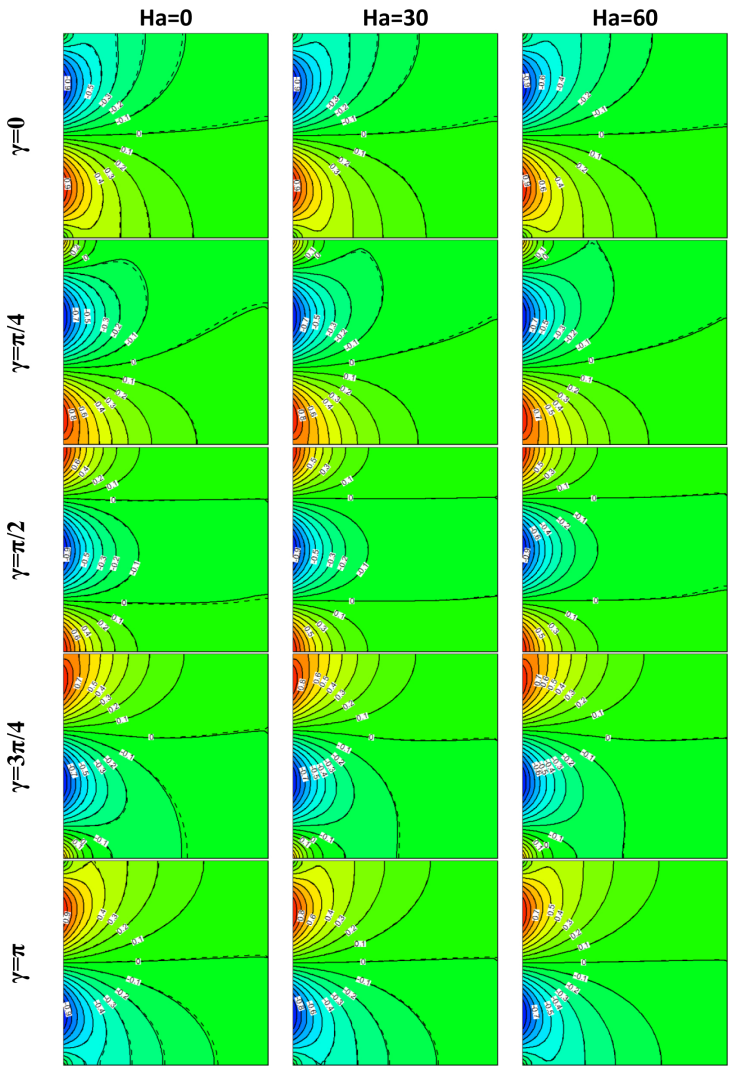

Figure 11: Isotherms for different Hartmann number and phase deviations for Ra $= 10^3$ (—) $\phi = 0.04$ and (- - -) $\phi = 0$

Fig.16a–b show the effect of the phase deviation respectively for Ra $= 10^3$ and 10^4 on the local Nusselt number for Ha $= 0$ and $\phi = 0$. For low Rayleigh number Ra $\leq 10^4$ (for both cases) it is observed that the local Nusselt number curves are approximately of sinusoidal shape like the thermal boundary along the left vertical walls. The local heat transfer is directly affected by the temperature distribution on the surface. Therefore, the higher heat transfer occurs in the higher temperature regions.

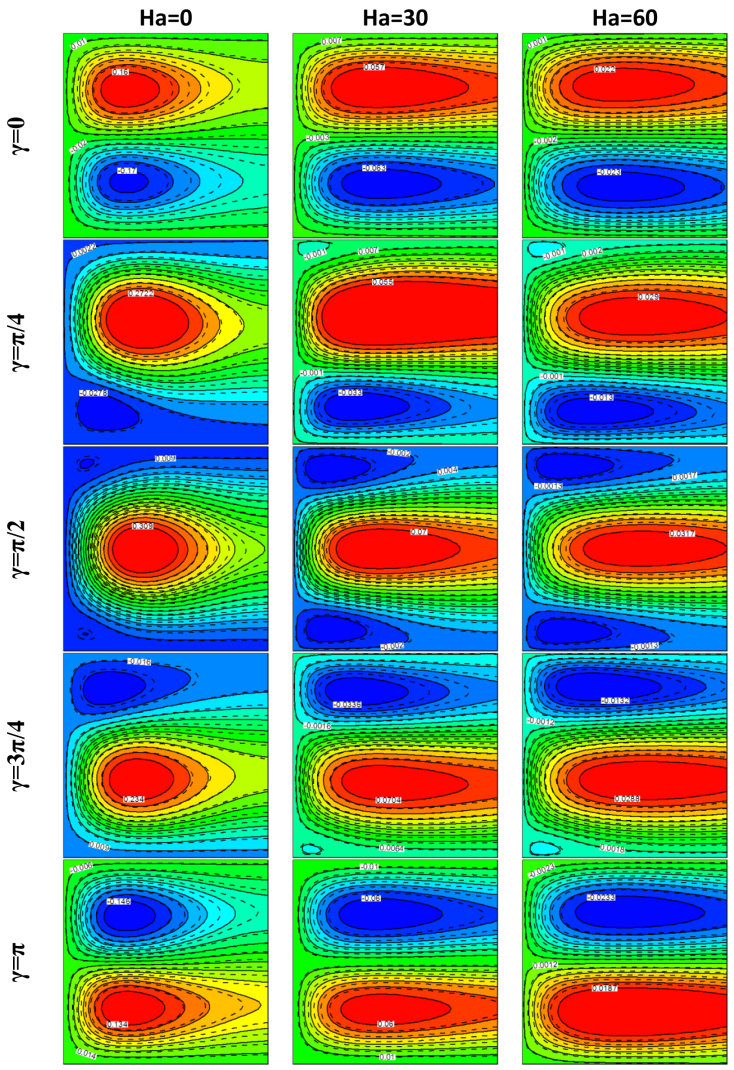

Figure 12: Streamlines for different Hartmann number and phase deviations for Ra $= 10^3$ (—) $\phi = 0.04$ and (- - -) $\phi = 0$

Fig.17a–b show the effect of the phase deviation respectively for Ha $= 0$ and 60 on the local Nusselt number for Ra $= 10^5$ and $\phi = 0$. By comparing **Fig. 16** and **17a**, it is shown that the local Nusselt number is greatly affected by high Rayleigh number (Ra $= 10^5$). Also, it is observed that the local Nusselt number increases with Rayleigh number. **Fig.17b** shows that the locale Nusselt number decreases with Hartmann number.

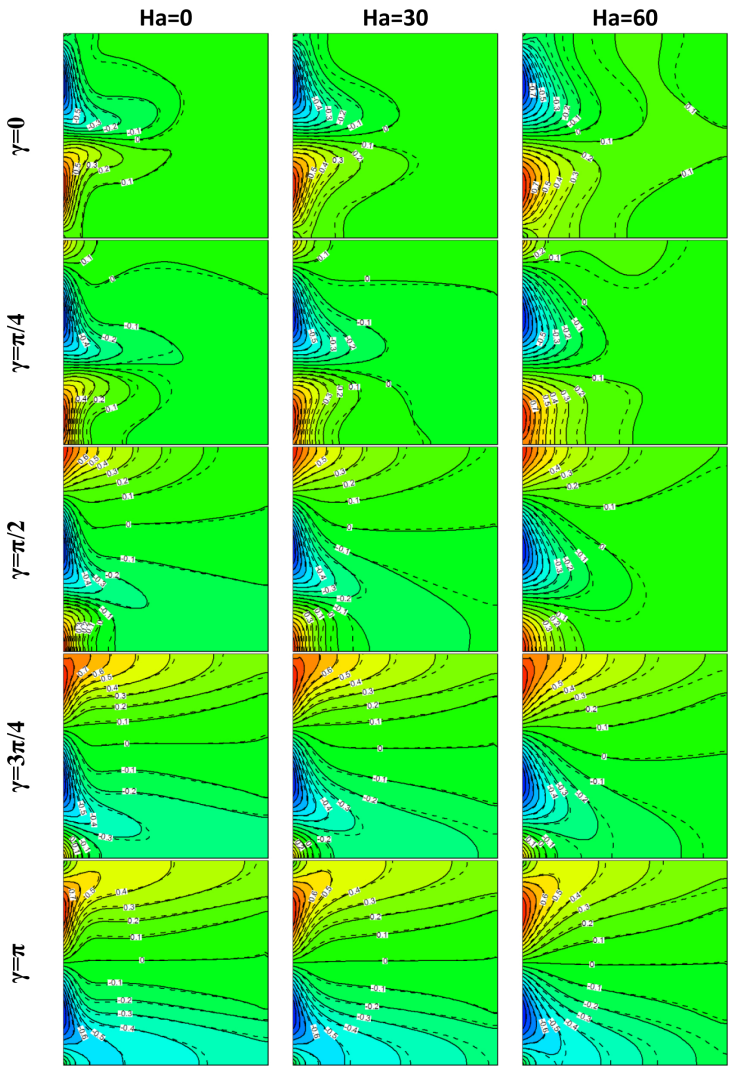

Figure 13: Isotherms for different Hartmann number and phase deviations for Ra $= 10^5$ (—) $\phi = 0.04$ and (- - -) $\phi = 0$

4.3 Effect of solid volume fraction

Fig. 18 shows the variation of the average Nusselt number as function of Hartmann number at different solid volume fraction, for Ra $= 10^5$ and $\gamma = \pi/2$. For all Hartmann number, the addition of nanoparticle increases the heat transfer rate.

Fig. 19 show the effect of the solid volume fraction on the average Nusselt number and the dimensionless average Nusselt number for Ha $= 30$, for different phase

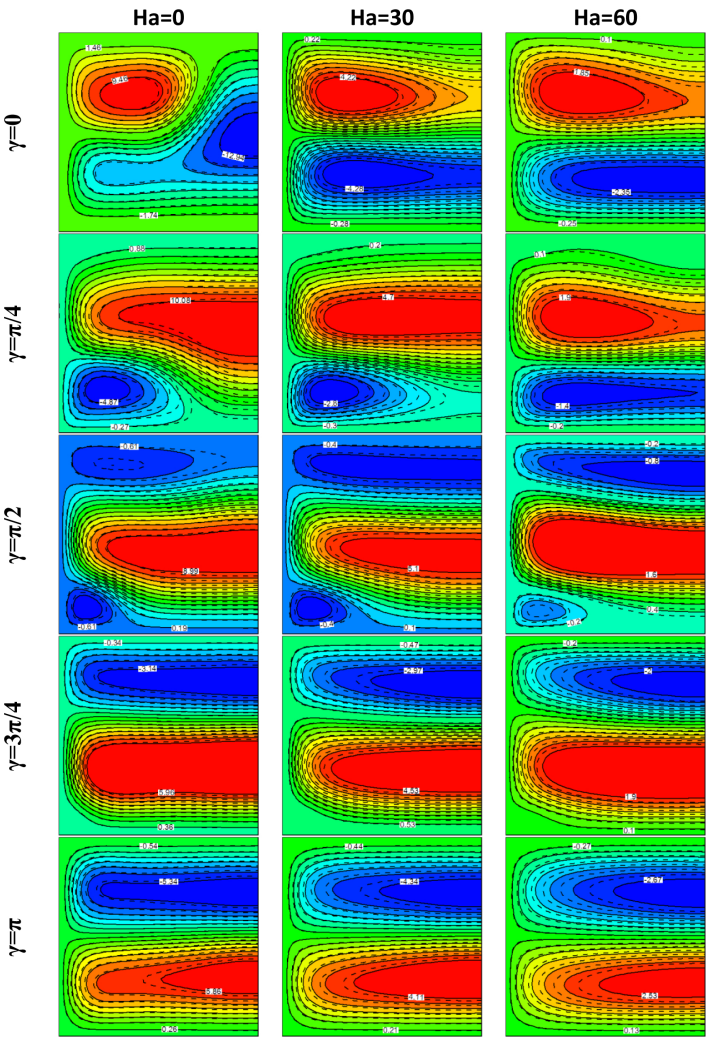

Figure 14: Streamlines for different Hartmann number and phase deviations for Ra $= 10^5$ (—) $\phi = 0.04$ and (- - -) $\phi = 0$

deviation and Rayleigh number. For low Rayleigh number (Ra $\leq 10^4$) the highest heat transfer rate is obtained for $\gamma = \pi/2$, the heat transfer increases from $\gamma = 0$ to $\pi/2$ and decreases from $\gamma = 3\pi/4$ to π. For Ra $= 10^3$the dimensionless average Nusselt number has the same behavior for the different phase deviations. While, for Ra $= 10^4$ the nanoparticle effect increases with the phase deviation. For Ra $= 10^5$, for $\gamma \geq \pi/4$ heat transfer increases with the phase deviations, the highest heat transfer rate is obtained in $\gamma = \pi$. The best effect of nanoparticles is obtained for $\gamma = \pi/2$.

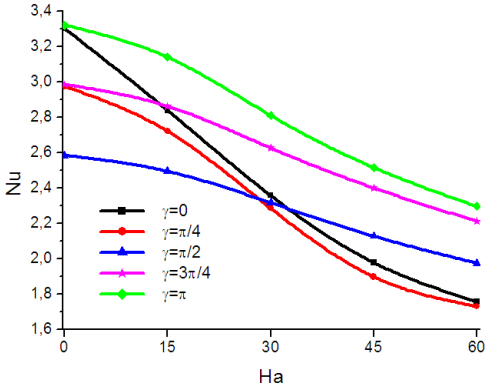

Figure 15: Variation of the average Nusselt number with Hartmann number for different phase deviation for Ra $= 10^5$ and $\phi = 0$

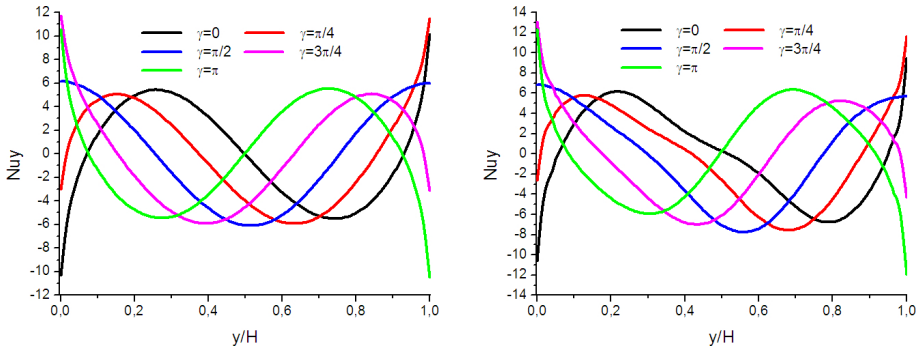

(a) (b)

Figure 16: Variation of the local Nusselt number on the left wall for different phase deviations for (a) Ra $= 10^3$ and (b) Ra $= 10^4$ at Ha $= 0$ and $\phi = 0$

5 Conclusions

In this paper the effects of the phase deviation, Rayleigh number, Hartmann number and solid volume fraction has been analyzed with Lattice Boltzmann Method. This study has been carried out for the pertinent parameters in the following ranges: Rayleigh number of base fluid, Ra $= 10^3$–10^6, Hartmann number between 0 and 60, phase deviation $\gamma = 0$, $\pi/4$, $\pi/2$, $3\pi/4$ and π and solid volume fraction from $\phi = 0$ to 0.06. This investigation was performed for various mentioned parameters and some conclusions were summarized as follows:

- A good agreement valid with previous numerical investigations demonstrates that Lattice Boltzmann Method is an appropriate method for different applicable problems.

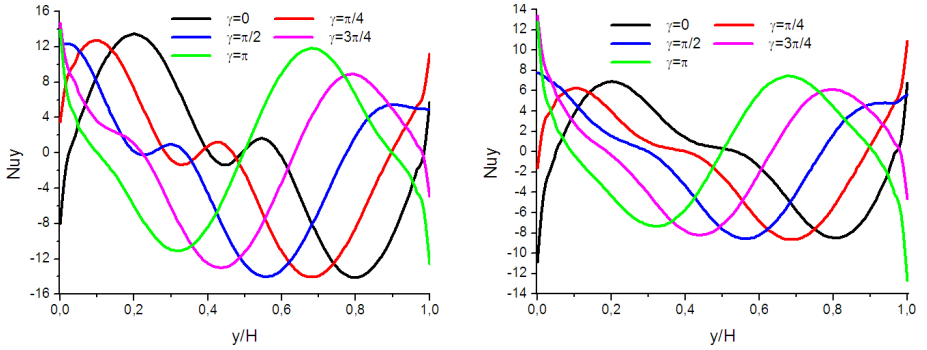

Figure 17: Variation of the local Nusselt number on the left wall for different phase deviations for (a) Ha = 0 and (b) Ha = 60 at Ra = 10^5 and $\phi = 0$

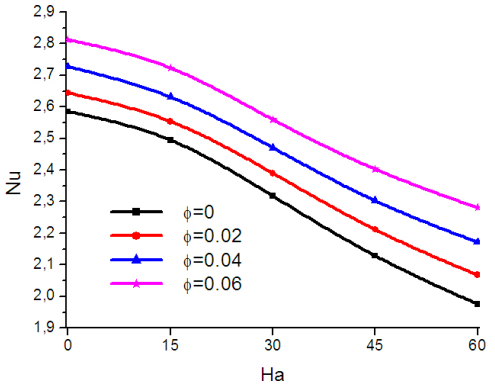

Figure 18: Variation of the average Nusselt number with Hartmann number for different solid volume fraction for Ra = 10^5 and $\gamma = \pi/2$

- The heat transfer rate decreases with the Hartmann number and increases with Rayleigh number.
- At Ra = 10^5, for $\gamma \geq \pi/2$, for Ha = 0 to 60, the heat transfer rate increases with the phase deviation.
- For all phase deviations the addition of nanoparticles increases heat transfer rate.
- For low Rayleigh number (Ra $\leq 10^4$) the highest heat transfer rate is obtained for $\gamma = \pi/2$.
- At Ra = 10^5, for $\gamma \geq \pi/4$ heat transfer increases with the phase deviations.
- At Ra = 10^5, the best effect of nanoparticles is obtained for $\gamma = \pi/2$.

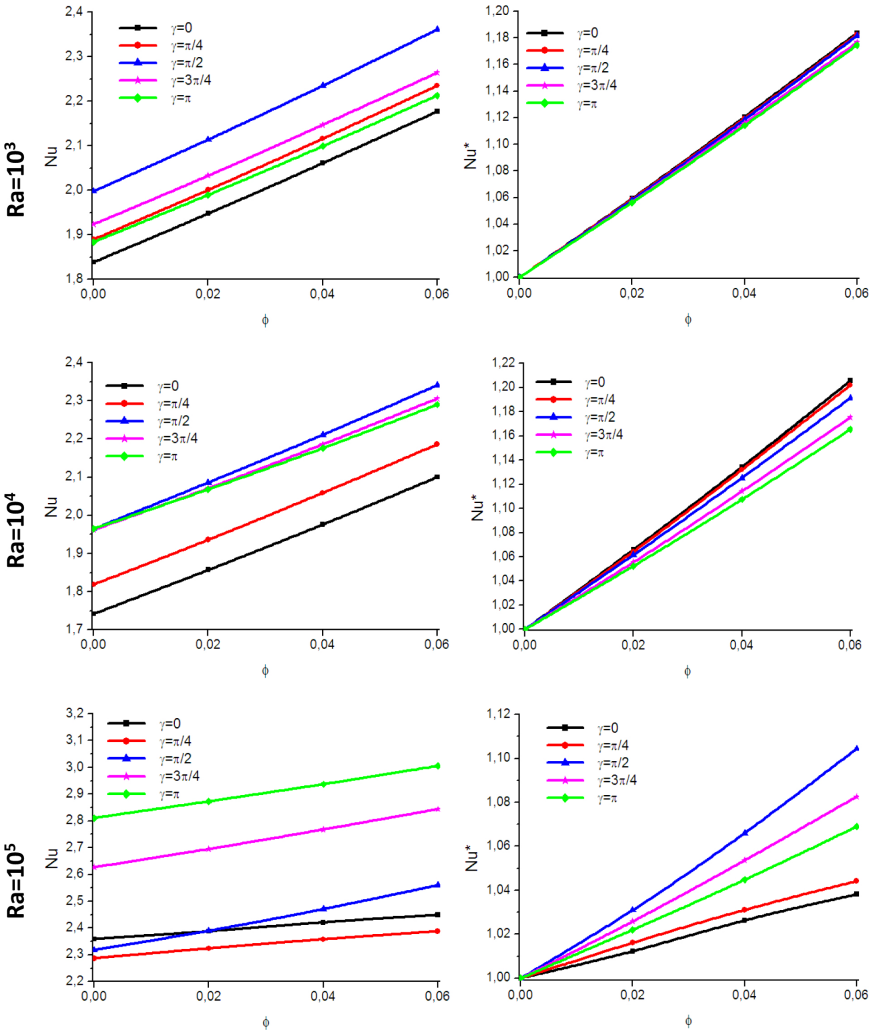

Figure 19: Variation of the average Nusselt number and dimensionless average Nusselt number with solid volume fraction for Ha = 30

References

Brinkman, H.C. (1952): The viscosity of concentrated suspensions and solution, *The Journal of Chemical Physics*, vol.20, pp. 571-581.

Chan, Y.L.; Tien, C.L. (1985): A numerical study of two-dimensional natural convection in square open cavities, *Numer. Heat Transfer*, vol. 8, pp. 65-80.

Fattahi, E.; Farhadi, M.; Sedighi, K.; Nemati, H. (2012): Lattice Boltzmann

simulation of natural convection heat transfer in nanofluids, *International Journal of Thermal Sciences*, vol.52, pp. 91-101.

Ghasemi, B.; Aminossadati, S.M.; Raisi, A. (2011): Magnetic field effect on natural convection in a nanofluid-filled square enclosure, *International Journal of Thermal Sciences*, vol.50, pp.1748-1756.

Jahanshahi, M.; Hosseinizadeh, S.F.; Alipanah, M.; Dehghani, A.; Vakilinejad G.R. (2010): Numerical simulation of free convection based on experimental measured conductivity in a square cavity using Water/SiO2 nanofluid, *International Communications in Heat and Mass Transfer*, vol.37, pp.687–694.

Kefayati, G.H.R. (2013): Lattice Boltzmann simulation of natural convection in partially heated cavities utilizing kerosene/ cobalt ferrofluid. *IJST, Transactions of Mechanical Engineering*, vol.37, pp. 107-118.

Kefayati, G.H.R.; Hosseinizadeh, S.F.; Gorji, M.; Sajjadi, H. (2012): Lattice Boltzmann simulation of natural convection in an open enclosure subjugated to water/copper nanofluid, *International Journal of Thermal Sciences*, vol. 52, pp. 91-101.

Kefayati, G.H.R.; Hosseinizaeh, S.F.; Gorji, M.; Sajjadi, H. (2011): Lattice Boltzmann simulation of natural convection in tall enclosures using water/SiO2 nanofluid, *International Communications in Heat and Mass Transfer*, vol.38, pp. 798-805.

Khanafer, K.; Vafai, K.; Lightstone, M. (2003): Buoyancy-driven heat transfer enhancement in a two-dimensional enclosure utilizing nanofluids, *International Journal of Heat and Mass Transfer*, vol.46, pp. 3639-3653.

Mahmoudi, A.; Mejri, I.; Abbassi, M.A.; Omri, A. (2014 a): Lattice Boltzmann simulation of MHD natural convection in a nanofluid-filled cavity with linear temperature distribution. *Powder Technology*, vol. 256, pp. 257–271.

Mahmoudi, A.; Mejri, I.; Abbassi, M.A.; Omri, A. (2014 b): Analysis ofMHD natural convection in a nanofluid-filled open cavitywith non uniform boundary condition in the presence of uniform heat generation/absorption. *Powder Technology*, vol. 269, pp. 275–289.

Mahmoudi, A.; Mejri, I.; Abbassi, M.A.; Omri, A. (2013): Numerical Study of Natural Convection in an Inclined Triangular Cavity for Different Thermal Boundary Conditions: Application of the Lattice Boltzmann Method, *Fluid Dyn. Mater. Processus*, vol. 9, n° 4, pp 353-388

Mahmoudi, A.H.; Shahi, M.; Shahedin, A.M.; Hemati, N. (2011): Numerical modeling of natural convection in an open enclosure with two vertical thin heat

sources subjected to a nanofluid, *International Communications in Heat and Mass Transfer*, vol. 38, pp.110–118.

Mejri, I.; Mahmoudi, A.; Abbassi, M.A.; Omri, A. (2014 a): Magnetic field effect on entropy generation in a nanofluid-filled enclosure with sinusoidal heating on both side walls, *Powder Technol*, vol.266, pp. 340-353.

Mejri, I.; Mahmoudi, A.; Abbassi, M.A.; Omri, A. (2014 b): MHD Natural Convection in a Nanofluid-filled Enclosure with Non-uniform Heating on Both SideWalls, *Fluid Dyn. Mater. Processus*, vol. 10, n° 1, pp 83-114

Mohamad, A.A.; Bennacer, R.; Ganaoui, M. (2010): Double dispersion, natural convection in an open end cavity simulation via Lattice Boltzmann Method, *International Journal of Thermal Sciences*, vol.49, pp. 1944-1953

Mohamad, A.A.; Ganaoui, M.; Bennacer, R. (2009): Lattice Boltzmann simulation of natural convection in an open ended enclosure, International Journal of Thermal Sciences, vol.48, pp.1870–1875.

Mohamad, A.A. (1995): Natural convection in open cavities and slots, *Numer. Heat Transfer*, vol. 27, pp. 705-716.

Maxwell, J.C. (1873): A Treatise on Electricity and Magnetism, vol. II, Oxford University Press, Cambridge, UK, pp. 54.

Quere, P.; Humphrey, J.A.C.; Sherman, F.S. (1981): Numerical calculation of thermally driven two-dimensional unsteady laminar flow in cavities of rectangular cross section, *Numer. Heat Transfer*, vol. 4, pp. 249-283.

Sheikholeslami, M.; Gorji-Bandpy, M.; Ganji, D.D.; Soleimani, S. (2014): Thermal management for free convection of nanofluid using two phase model, *Journal of Molecular Liquids*, vol.194, pp. 179–187.

Xuan, Y.; Roetzel, W. (2000): Conceptions for heat transfer correlation of nanofluids, *International Journal of Heat and Mass Transfer*, vol.43, pp. 3701-3707.